J. Fluid Mech. (1997), *vol.* 352, *pp.* 305–330. Printed in the United Kingdom

Thermocapillary flow in a Hele-Shaw cell

By W. BOOS AND A. THESS

Center for Physical Fluid Dynamics, Department of Mechanical Engineering,
Dresden University of Technology, 01062 Dresden, Germany

(Received 12 July 1996 and in revised form 11 August 1997)

We formulate a simple theoretical model that permits one to investigate surface-tension-driven flows with complex interface geometry. The model consists of a Hele-Shaw cell filled with two different fluids and subjected to a unidirectional temperature gradient. The shape of the interface that separates the fluids can be arbitrarily complex. If the contact line is pinned, i.e. unable to move, the problem of calculating the flow in both fluids is governed by a linear set of equations containing the characteristic aspect ratio and the viscosity ratio as the only input parameters. Analytical solutions, derived for a linear interface and for a circular drop, demonstrate that for large aspect ratio the flow field splits into a potential core flow and a thermocapillary boundary layer which acts as a source for the core. An asymptotic theory is developed for this limit which reduces the mathematical problem to a Laplace equation with Dirichlet boundary conditions. This problem can be efficiently solved utilizing a boundary element method. It is found that the thermocapillary flow in non-circular drops has a highly non-trivial streamline topology. After releasing the assumption of a pinned interface, a linear stability analysis is carried out for the interface under both transverse and longitudinal temperature gradients. For a semi-infinite fluid bounded by a freely movable surface long-wavelength instability due to the temperature gradient across the surface is predicted. The mechanism of this instability is closely related to the long-wave instability in surface-tension-driven Bénard convection. A linear interface heated from the side is found to be linearly stable. The possibility of experimental verification of the predictions is briefly discussed.

1. Introduction

When the temperature at the interface between two immiscible fluids is not uniform, a flow may be induced due to the temperature dependence of surface tension (Davis 1987). This flow is usually called thermocapillary convection or Marangoni convection. It plays an important role in Bénard convection in shallow fluid layers (Koschmieder 1993), in chemical engineering (Edwards, Brenner & Wasan 1991), as well as in crystal growth and other materials processing technologies (Hammerschmid 1987).

Theoretical and experimental study of thermocapillary flow is difficult for two reasons. On the one hand, thermocapillary flow involves a delicate interplay between the inherent nonlinearity of the basic equations of fluid dynamics and the dynamics of the phase boundary with complex geometry. On the other hand, thermocapillary flow on Earth is usually accompanied by buoyancy-driven convection. Hence, observation of the former in its pure form is nearly impossible.

The goal of the present work is to propose a simple, yet experimentally realizable,

model that permits us to study pure thermocapillary convection in complex geometries. We shall focus on the Stokes flow regime, where nonlinearities of the governing equations can be neglected. This assumption permits, to the greatest possible extent, the separation of the aspect of complex interface shape from the complexity due the nonlinearity of the basic equations. Moreover, the two-dimensionality of the system provides the opportunity of making the flow perpendicular to the gravity field, thereby permitting one to study thermocapillary flow isolated from the influence of buoyancy under terrestrial conditions.

An additional motivation for the investigation of linearized thermocapillary flow in complex geometries comes from the observation that boundary integral techniques which have proved extremely useful in ordinary (isothermal) viscous flows (Pozrikidis 1992) have not been applied to thermocapillary problems yet, although there is good reason to believe that such application would be of considerable interest. For instance, a profound understanding of pulmonary flow (i.e. flow in the lungs of humans and land animals, see Grotberg 1994 for a review) requires, among other things, a modelling of surface-tension-driven flows in the complex shaped alveoli (the terminal air sacs in which the diffusional gas exchange takes place) due to surfactants. Since surfactants play an analogous role in modifying the surface tension to the temperature field, and since the Reynolds number is often small, boundary integral techniques can be used to treat the important problem of surfactant spreading (Jensen & Grotberg 1992) in more realistic complex geometries than the planar one. From the fundamental viewpoint, boundary integral techniques are deemed appropriate to extend our understanding of the long-wave instability in surface-tension-driven Bénard convection (VanHook *et al.* 1995) beyond linear stability theory (Scriven & Sternling 1964) and weakly nonlinear model equations (Davis 1983, 1987) by taking into account strong surface deformations. Before tackling the complex three-dimensional problems mentioned above, it is desirable to formulate and test boundary integral techniques for thermocapillary flows using prototype problems of which the present model is likely to be the simplest non-trivial representative.

The system under consideration, to be defined in the following section, is a generalization of previous experimental and theoretical work by Siekmann (1979) and Bratuhin & Zuev (1984). Their model consists of two fluids enclosed in a narrow gap between two parallel horizontal plates (Hele-Shaw cell) subject to a uniform horizontal temperature gradient. The main difference from the previous work consists in the assumption that the phase boundary between the two fluids can have arbitrarily complex shape. In §3 we derive the set of equations governing the thermocapillary flow in a Hele-Shaw cell. Section 4 contains exact solutions of the equations for the case of a linear interface and for a circular drop. In §5 we develop an asymptotic theory appropriate to the modelling of large-aspect-ratio structures. Furthermore, in §6, we apply the theory to non-circular drops with two-fold and four-fold symmetry, using the boundary element method. Section 7 addresses some questions of surface-wave instabilities for the particular case of non-wetting fluid. In §8 we summarize our conclusions and discuss the possibility of experimental verification of our theoretical predictions.

Before embarking on a systematic treatment of the problem, it is useful to summarize briefly previous work on surface-tension-driven flow in complex geometries. The subject of steady thermocapillary-driven motion of a single spherical droplet in an unbounded fluid subject to a constant temperature gradient was first addressed in the work of Young, Goldstein & Block (1959). Later on, this problem was extended to deformable droplets by Bratuhin (1975) and to time-dependent flow by Galindo *et al.* (1994). One particular problem, namely the steady thermocapillary-driven motion of

a large droplet contained in a tube, was analysed by Wilson (1993). Another aspect of surface-tension-driven flow was studied by Ehrhard & Davis (1991), who investigated the spreading of liquid drops on horizontal plates subject to capillary, thermocapillary and gravity forces. This list of works and authors can be extended.

The classical Hele-Shaw problem with *constant* surface tension has been and is still being intensively studied in the context of pattern formation, nonlinear interface dynamics, and formation of singularities. We refer the reader to the work of Bensimon *et al.* (1986) for an introductory review. Less is known about thermocapillary-driven flow in Hele-Shaw cells. Siekmann (1979) has presented a theory of slow motion of a circular bubble subject to a horizontal temperature gradient. However, experiments of Bratuhin & Zuev (1984) did not show convincing agreement with that theory – a question that will be discussed in the light of our results in the last section.

In a recent experimental work on bubble motion in a Hele-Shaw cell Bush (1997) has identified a novel wake structure characterized by an intense jet produced by surface-tension gradients. It will be shown below that this can be partly understood in the framework of the present theory (although a three-dimensional analysis would be necessary to describe completely the reported experiments).

2. Definition of the system

We consider two immiscible viscous fluids confined in a Hele-Shaw cell formed by two parallel plates with separation h, as sketched in figure 1(a). In contrast to previous studies of Siekmann (1979) and Bratuhin & Zuev (1984) which were focused on a bubble in a wetting fluid (see figure 1(b)), we are interested here in a situation sketched in figure 1(c) where the interface possesses two contact lines. Moreover, we shall suppose that the contact lines are unable to move. Such behaviour, often referred to as pinning (de Gennes 1985), is the macroscopic manifestation of microscopic fluctuations in the mechanical or chemical properties of the plates. For our purpose it is sufficient to note that pinning of contact lines can be achieved by endowing the plates with artificial roughness on a microscopic scale. The assumption of a pinned contact line permits one to study flows with arbitrarily complex interface shape without the need to consider their dynamical evolution. In the §7 where movable interfaces are considered we shall make some necessary comments about the dynamics of contact lines.

Let the Hele-Shaw cell be arranged perpendicular to the gravity field such that buoyancy has no influence on the interface shape and on the motion of the fluids – a condition that will be made more precise in the next section. Furthermore the system is heated at one side and cooled at the other so that the plates are subject to a constant horizontal temperature gradient.

The distance between the plates is supposed to be sufficiently small for the imposed temperature gradient to extend into the fluid without modification, which is equivalent to the assumption of small Péclet number (for details see the Appendix). Since the temperature field within the fluid is not constant, a flow is induced at the interface between the fluids whose surface tension α is assumed to depend on temperature. For most fluids, surface tension decreases with increasing temperature, and the dependence of surface tension on temperature can be approximately written in the linear form

$$\alpha = \alpha_o - \gamma(T - T_o), \tag{2.1}$$

where the mostly positive coefficient $\gamma = -\partial\alpha/\partial T$ is called the thermal coefficient of surface tension, and T is temperature. The resulting flow is called thermocapillary flow.

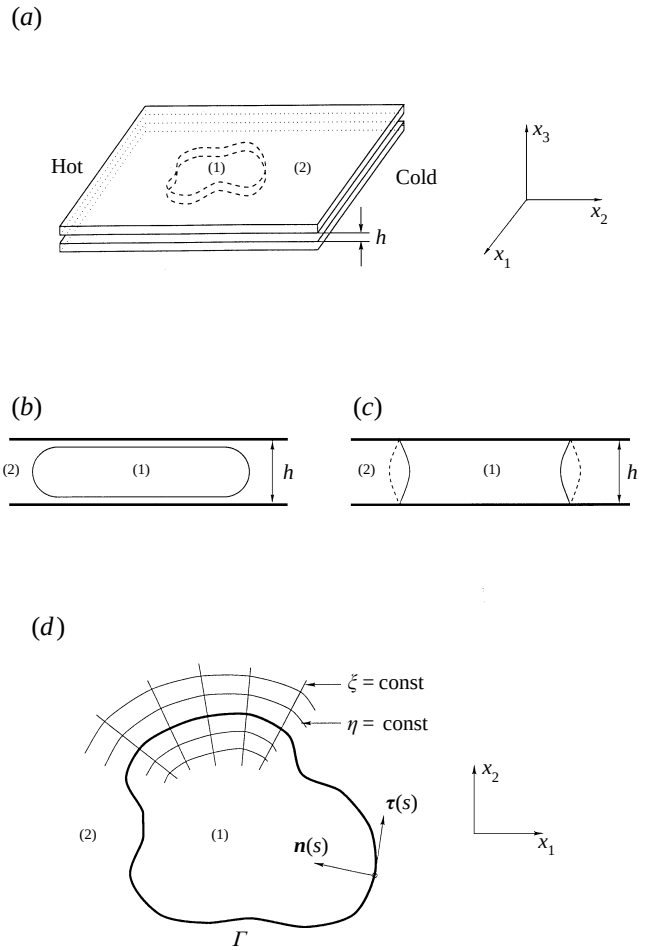

FIGURE 1. Thermocapillary flow in a Hele-Shaw cell: (*a*) a sketch of the problem considered, (*b*) a system without a contact line, as opposed to a system (*c*) involving contact lines as considered in the present work, (*d*) a sketch of the curvilinear coordinate system.

3. Mathematical formulation of the problem

We arrange the cell perpendicular to the gravity force and introduce an orthogonal coordinate system (x_1, x_2, x_3) with basis unit vectors $(\boldsymbol{e}_1, \boldsymbol{e}_2, \boldsymbol{e}_3)$. Here the x_3-axis is vertical to the plane of the cell and opposite to the direction of gravity. The coordinates (x_1, x_2) are in the plane of the cell and the origin is chosen to be at the interface between the bottom plate ($x_3 = 0$) and the fluid. The top plate is then located at $x_3 = h$. Throughout this work we label one fluid as (1), and the other as (2) and denote the corresponding quantities by superscripts (1) or (2). If equations are valid for both fluids, we will omit the superscript.

Both plates, which are supposed to have high thermal conductivity, are subjected to a homogeneous horizontal temperature gradient of the form

$$T = T_o + \beta(\boldsymbol{t} \cdot \boldsymbol{x}), \tag{3.1}$$

where β is the absolute value of temperature gradient and $\boldsymbol{t}$ represents the unit vector in the direction of the temperature gradient.

Our mathematical model rests on the following three assumptions.

First, we assume that the distance h between the plates is sufficiently small for gravity to have negligible influence on the shape of the interface. In this case the ratio $h^2/a^2 < 1$ between the distance h and the capillary constant $a^2 = 2\alpha/\rho g$ is small. This condition expresses the fact that the pressure forces due to surface tension $p_\alpha \sim \alpha/h$ should be sufficiently strong to prevent the hydrostatic pressure difference $p_g \sim | \rho_1 - \rho_2 | gh$ from allowing the heavy fluid (density ρ_1) to displace the light fluid (density ρ_2) towards the top plate. For example, if we take a Hele-Shaw cell with depth $h = 1$ mm and silicone oil NM 10 we have $h^2/a^2 \approx 0.25$, $p_s \approx 15.2$ Pa, $p_g \approx 7.5$ Pa, and the condition is satisfied.

Second, we shall assume that the Reynolds number $Re = uh/v$ evaluated with the thermocapillary velocity scale $u = \gamma\beta h/\mu$, which is the relevant velocity of the problem at hand, is small. Here v and $\mu = \rho v$ denote the kinematic and dynamic viscosity respectively. Indeed, for our previous example with $\beta = 100$ K m^{-1} we obtain $u \sim 0.63$ mm s^{-1} and $Re = 6.3 \times 10^{-3}$. This assumption permits us to use the linear Stokes equation instead of the nonlinear Navier–Stokes equation for the description of the flow.

Third, we suppose that the temperature gradient (3.1) imposed along the plates is passed into the fluids without being affected by the different heat conductivities of the fluids and their motion. The neglect of fluid motion is justified if heat diffusion dominates over heat advection – a condition that is expressed by the smallness of the Péclet number $Pe = uh/\kappa$ where κ is the heat diffusivity of the fluid. This condition can always be achieved by choosing sufficiently small thickness h. In our previous example with silicone oil $Pe < 1$ if $h < 0.2$ mm. Note that, even at zero Péclet number, the temperature of the fluids will in general differ from that of the plates due to the finite heat conductivities of the fluids. However, it will be shown in the Appendix that even for the worst case, when the heat conductivity of one fluid is zero, the departure of the mean temperature $\langle T \rangle = h^{-1} \int T \mathrm{d}z$ of the other fluid from the imposed temperature (3.1) is always smaller than $\beta h/\pi$. It is thereby of the same order as other terms, neglected in the course of the derivation of the equations of Hele-Shaw flow.

3.1. *Governing equations*

Under the conditions $Ca = \mu u/\alpha \ll 1$ (small Capillary number), $Re \ll 1$, and $Pe \ll 1$ formulated above, the motion of the incompressible fluids can be described by the Stokes equation

$$\nabla p = \mu \Delta \boldsymbol{V}, \tag{3.2}$$

where p is the pressure and $\boldsymbol{V}$ is the fluid velocity field. In addition, we have for each liquid the mass conservation equation

$$\operatorname{div} \boldsymbol{V} = 0, \tag{3.3}$$

We use the same method for converting the three-dimensional equations (3.2), (3.3) into a two-dimensional model as is done in the classical Hele-Shaw problem, namely averaging over the height h of the cell. For that purpose we assume the velocity field to be of the form

$$\boldsymbol{V}(x_1, x_2, x_3) = \boldsymbol{v}(x_1, x_2) w(x_3), \tag{3.4}$$

where $\boldsymbol{v} = v_1 \boldsymbol{e}_1 + v_2 \boldsymbol{e}_2$ represents the unknown two-dimensional velocity field in the cell and $w(x_3) = 6(x_3 h - x_3^2)/h^2$ is a single scalar function which describes the Poiseuille profile of the velocity over the height of the cell. An evaluation of the x_3-component

of the Stokes equation with the velocity field (3.4) leads to the condition $\partial p/\partial z = 0$. Thus the pressure is a function of the horizontal coordinates only. Observe that the independence of p of the vertical coordinate is a consequence of the assumption that the vertical velocity vanishes.

Inserting (3.4) into the Stokes equation (3.2) and continuity equation (3.3) and averaging by integrating with respect to x_3, we obtain the equations for pressure p and two-dimensional velocity $\boldsymbol{v}$ as

$$\nabla p = \mu \left(\Delta \boldsymbol{v} - k^2 \boldsymbol{v}\right), \tag{3.5}$$

$$\operatorname{div} \boldsymbol{v} = 0, \tag{3.6}$$

where $k^2 = 12/h^2$. Looking at equation (3.5) one can see that it differs from the two-dimensional Stokes equation by the additional dissipative term $-k^2\boldsymbol{v}$. This term may be interpreted as the average friction force due to the presence of the plates. By omitting the term $\Delta\boldsymbol{v}$, we would obtain the so-called Darcy approximation of the Navier–Stokes equation, which is often used for the consideration of fingering in Helle-Shaw cells, penetration into porous media, etc., and describes potential flow. By contrast, in our case the presence of the second-order term is crucial, because the thermocapillary flow is driven by shear stresses and can therefore in general not be potential.

For two-dimensional flows it is convenient to rewrite the problem in terms of the streamfunction $\Psi(x_1, x_2)$ defined by

$$\boldsymbol{v} = \operatorname{rot}(\Psi \boldsymbol{e}_3),$$

which automatically satisfies the incompressibility constraint. The equation for Ψ is obtained by taking the curl of (3.5) and has the form

$$\Delta\left(\Delta - k^2\right)\Psi = 0. \tag{3.7}$$

Once Ψ is known, the pressure can be calculated by solving the Poisson equation

$$\Delta p = 0, \tag{3.8}$$

with the boundary condition

$$\nabla p = \mu \operatorname{rot}(\Delta - k^2)\Psi \boldsymbol{e}_3. \tag{3.9}$$

3.2. *Curvilinear coordinate system*

We introduce a curvilinear coordinate system, which is adjusted to the interface. This coordinate system contains all the information about the geometry of the interface and will be useful to formulate the boundary conditions in an invariant form.

The projection of the interface between the two fluids onto the (x_1, x_2)-plane gives a curve Γ. It is assumed that this curve has no singularities. The curve can be either closed (if we consider a droplet in a liquid), or open (if both liquids are unbounded). Let the curve Γ be described by the vector function $\boldsymbol{X}(s) = X_1(s)\boldsymbol{e}_1 + X_2(s)\boldsymbol{e}_2$ parametrized in terms of the arclength s along Γ. The orientation of Γ is chosen such that liquid (1) is on the left side when moving along Γ in the direction of increasing s. Furthermore we introduce the unit tangential vector $\boldsymbol{\tau}(s) = \mathrm{d}\boldsymbol{X}/\mathrm{d}s$, the unit normal vector $\boldsymbol{n}(s) = \boldsymbol{e}_3 \times \boldsymbol{\tau}$, and the curvature $K(s) = |\mathrm{d}^2\boldsymbol{X}/\mathrm{d}s^2|$.

We define a curvilinear coordinate system (ξ, η) with the unit vectors $(\boldsymbol{\tau}, \boldsymbol{n})$ by the transformation

$$x_1 = X_1(\xi) + (\boldsymbol{n} \cdot \boldsymbol{e}_1)\eta, \quad x_2 = X_2(\xi) + (\boldsymbol{n} \cdot \boldsymbol{e}_2)\eta, \tag{3.10}$$

which characterizes each point (x_1, x_2) by the location ξ of its projection onto the phase boundary and by its distance η from Γ. The structure of this local coordinate system is sketched in figure 1(*d*). For $\eta = 0$ the coordinate ξ is equivalent to the arclength s along the interface. The reader can easily verify that the coordinate system is orthogonal.

The curvilinear scale factors, called Lamé's coefficients, are then

$$\ell_1 = 1 - (\boldsymbol{n} \cdot \mathrm{d}^2\boldsymbol{X}/\mathrm{d}s^2)\eta \text{ and } \ell_2 = 1.$$

In what follows $\ell(s)$ will be used to specify the non-trivial first Lamé coefficient. For details of the derivation of (3.10) and the curvilinear scale factors the reader is referred to Aris (1989). In general, the coordinate system (ξ, η) is non-singular only in a thin layer around the curve $(-\max_s |K(s)| \leqslant \eta \leqslant \max_s |K(s)|)$. However, this is sufficient for our analysis since the main purpose of the introduction of ξ and η is to formulate the boundary conditions and an asymptotic boundary-layer theory in the immediate vicinity of the interface.

To conclude this section we write down the explicit expressions for the velocity components and the Laplacian

$$v_\xi = \frac{\partial \Psi}{\partial \eta}, \qquad v_\eta = -\frac{1}{\ell}\frac{\partial \Psi}{\partial \xi}, \tag{3.11}$$

$$\Delta = \frac{1}{\ell}\left(\frac{\partial}{\partial \xi}\frac{1}{\ell}\frac{\partial}{\partial \xi} + \frac{\partial}{\partial \eta}\ell\frac{\partial}{\partial \eta}\right). \tag{3.12}$$

3.3. *Boundary conditions*

The basic kinematic and dynamic conditions on any material fluid boundary Γ ensure the continuity of both velocity and shear stress with allowance for surface tension. We denote the jump of any quantity g across Γ as $[g]$, so that for instance $[\boldsymbol{v}] = \boldsymbol{v}^{(1)} - \boldsymbol{v}^{(2)}$ on Γ. Since the interface is pinned, the normal velocity components must vanish at Γ, which is expressed by

$$\boldsymbol{n} \cdot \boldsymbol{v} = 0. \tag{3.13}$$

The continuity of tangential velocity requires

$$[\boldsymbol{\tau} \cdot \boldsymbol{v}] = 0. \tag{3.14}$$

Continuity of shear stress implies

$$[\boldsymbol{\tau} \cdot \boldsymbol{\sigma} \cdot \boldsymbol{n}] = -\nabla\alpha, \tag{3.15}$$

where $\boldsymbol{\sigma}$ is the stress tensor with components

$$\sigma_{ij} = -p\delta_{ij} + \mu\left(\frac{\partial v_i}{\partial x_j} + \frac{\partial v_j}{\partial x_i}\right), \tag{3.16}$$

$(i, j = 1, 2)$ and α is the surface tension. At infinity the outer fluid is at rest, i.e.

$$\lim_{\eta \to \infty} \boldsymbol{v} = 0, \tag{3.17}$$

where η is distance from interface. Inserting (2.1), (3.1), (3.11), into (3.14)–(3.17) we

find the boundary conditions for the streamfunction Ψ in the coordinate system (ξ, η), as

$$\frac{\partial \Psi}{\partial \xi} = 0 \qquad \text{at } \eta = 0, \tag{3.18}$$

$$\left[\frac{\partial}{\partial \eta}\Psi\right] = 0 \qquad \text{at } \eta = 0, \tag{3.19}$$

$$\left[\mu \ell \frac{\partial}{\partial \eta}\frac{1}{\ell}\frac{\partial \Psi}{\partial \eta}\right] = \gamma\,\beta\,(\boldsymbol{\tau}\cdot\boldsymbol{t}) \qquad \text{at } \eta = 0, \tag{3.20}$$

$$\lim_{\eta\to\infty} \Psi = \text{Const}, \tag{3.21}$$

with γ denoting a positive constant. Since Ψ is only determined up to an arbitrary constant, (3.18) is equivalent to the requirement that $\Psi^{(1)} = \Psi^{(2)} = 0$ on Γ.

3.4. *Dimensionless form*

We scale the spatial coordinates (x_1, x_2) as well as (ξ, η) by the length scale L which characterizes the lateral extent of the object under consideration. In the absence of a lateral scale, such as for the particular case of a straight interface between two semi-infinite fluids, we shall use $L = h$. Distinguishing the new dimensionless variables with a tilde we have

$$x_1 = L\tilde{x}_1, \quad x_2 = L\tilde{x}_2, \quad \xi = L\tilde{\xi}, \quad \eta = L\tilde{\eta}. \tag{3.22}$$

Since the convection is a balance between thermocapillary stresses proportional to $\gamma\beta$ and the viscous stresses proportional to $\mu v/L \sim \mu\Psi/L^2$, we can introduce a dimensionless streamfunction and viscosity according to

$$\Psi = \frac{\gamma\beta L^2}{\mu^{(1)} + \mu^{(2)}}\tilde{\Psi}, \tag{3.23}$$

$$\mu = (\mu^{(1)} + \mu^{(2)})\tilde{\mu}. \tag{3.24}$$

Introducing $k = L^{-1}\tilde{k}$ (which is equivalent to $\tilde{k}^2 = 12L^2/h^2$) and dropping the tilde in all quantities we can write down the governing equations for both fluids in dimensionless form as

$$\Delta\left(\Delta - k^2\right)\Psi = 0. \tag{3.25}$$

The boundary conditions (3.18)–(3.21) become

$$\Psi = 0 \qquad \text{at } \eta = 0, \tag{3.26}$$

$$\left[\frac{\partial}{\partial \eta}\Psi\right] = 0 \qquad \text{at } \eta = 0, \tag{3.27}$$

$$\left[\mu \ell \frac{\partial}{\partial \eta}\frac{1}{\ell}\frac{\partial \Psi}{\partial \eta}\right] = (\boldsymbol{\tau}\cdot\boldsymbol{t}) \qquad \text{at } \eta = 0, \tag{3.28}$$

$$\Psi = \text{Const} \qquad \text{as } \eta \to \infty. \tag{3.29}$$

The dimensionless system (3.25)–(3.29) contains two parameters, namely the aspect ratio $k = \sqrt{12}L/h$ and the viscosity ratio $\hat{\mu} = \mu^{(1)}/(\mu^{(1)} + \mu^{(2)})$. For a given curve Γ and the associated Lamé coefficient $\ell(s)$ the system completely determines the stream functions in both fluids.

If $\hat{\mu} = 0$ then fluid (1) is inviscid and can be associated with air. On the other hand, if $\hat{\mu} = 1$ then fluid (2) is inviscid. In these two limiting cases our problem can

be solved only for the viscous fluid because for inviscid fluids the Reynolds number is not limited ($Re \to \infty$) and the Stokes approximation is not valid.

4. Analytical solutions

For the particular cases of a linear interface and for circular drops and bubbles the system (3.25)–(3.29) has exact analytic solutions. These solutions provide a useful key for the qualitative understanding of flows in more complex geometries to be considered in §6.

4.1. *Linear interface*

Consider two semi-infinite fluids bounded by a common linear interface $x_2 = 0$ which are exposed to a temperature gradient along the interface. We choose the coordinates (x_1, x_2) as Cartesian coordinates (x, y) with the x-axis oriented in the direction of the temperature gradient ∇T, so that the first liquid is above and second liquid below the x-axis. Since the only available length scale of the problem is the height of the cell, we use $L = h$, which leads to $k^2 = 12$. Using the fact that $\ell(s) = 1$, $\boldsymbol{\tau} \cdot \boldsymbol{t} = 1$ and assuming that the flow is independent of x, we are left with the equation

$$\left(\frac{\mathrm{d}^2}{\mathrm{d}y^2} - 12\right)\frac{\mathrm{d}^2\Psi}{\mathrm{d}y^2} = 0 \tag{4.1}$$

for the streamfunctions in both fluids and with the boundary conditions

$$\Psi^{(1)} = \Psi^{(2)} = 0, \tag{4.2}$$

$$\frac{\mathrm{d}\Psi^{(1)}}{\mathrm{d}y} = \frac{\mathrm{d}\Psi^{(2)}}{\mathrm{d}y}, \tag{4.3}$$

$$(1-\hat{\mu})\frac{\mathrm{d}^2\Psi^{(2)}}{\mathrm{d}y^2} - \hat{\mu}\frac{\mathrm{d}^2\Psi^{(1)}}{\mathrm{d}y^2} = 1, \tag{4.4}$$

at $y = 0$. The solution to this problem is easily found as

$$\Psi^{(1)} = \frac{\mathrm{e}^{-\sqrt{12}y} - 1}{12}, \tag{4.5}$$

$$\Psi^{(2)} = \frac{1 - \mathrm{e}^{\sqrt{12}y}}{12}. \tag{4.6}$$

This solution corresponds to the velocity field

$$v_x^{(1)} = -\frac{\mathrm{e}^{-\sqrt{12}y}}{\sqrt{12}}, \tag{4.7}$$

$$v_x^{(2)} = -\frac{\mathrm{e}^{\sqrt{12}y}}{\sqrt{12}} \tag{4.8}$$

(and $v_y = 0$), which describes a unidirectional flow along the interface which is directed towards the cooled side and decays exponentially with increasing distance from the interface. Observe that the spatial decay rate is equal in both fluids, owing to the absence of any characteristic length scale in the problem other than the plate separation. Moreover, it is worth noting that the solution does not contain the viscosity ratio, which disappears from the boundary conditions (4.4) on account of the symmetry of the streamfunction.

The linear interface is a useful model to assess the quality of the two-dimensional approximation because it admits an exact three-dimensional solution as we show next.

In order to solve the three-dimensional Stokes problem (3.2), (3.3) we assume zero pressure gradient along the interface and a velocity field of the form $\boldsymbol{V} = U_x(y,z)\boldsymbol{e}_x$. The continuity equation is then automatically satisfied, and the Stokes equation transforms into the Poisson equation

$$\Delta U_x = 0. \tag{4.9}$$

The no-slip boundary condition at the upper and lower plates reads

$$U_x(y,0) = U_x(y,1) = 0, \tag{4.10}$$

while the three-dimensional version of the Marangoni boundary condition (3.15) takes the form

$$(1-\hat{\mu})\frac{\partial U_x^{(2)}(0,z)}{\partial y} - \hat{\mu}\frac{\partial U_x^{(1)}(0,z)}{\partial y} = 1. \tag{4.11}$$

A straightforward calculation provides the exact solution

$$U_x^{(1)} = -\frac{4}{\pi^2}\sum_{n=1}^{\infty}\frac{\mathrm{e}^{-\pi(2n-1)y}}{(2n-1)^2}\sin[\pi(2n-1)z],$$

$$U_x^{(2)} = -\frac{4}{\pi^2}\sum_{n=1}^{\infty}\frac{\mathrm{e}^{\pi(2n-1)y}}{(2n-1)^2}\sin[\pi(2n-1)z],$$

for the velocity fields in both fluids. In order to compare with the two-dimensional model we average these expressions with respect to z and obtain

$$\bar{U}_x^{(1)} = -\frac{8}{\pi^3}\sum_{n=1}^{\infty}\frac{\mathrm{e}^{-\pi(2n-1)y}}{(2n-1)^3}, \tag{4.12}$$

$$\bar{U}_x^{(2)} = -\frac{8}{\pi^3}\sum_{n=1}^{\infty}\frac{\mathrm{e}^{\pi(2n-1)y}}{(2n-1)^3}, \tag{4.13}$$

where the bar denotes averaged value. Now we can compare the averaged three-dimensional solutions (4.12), (4.13) with the solutions (4.7), (4.8). Since the solutions are symmetric figure 2 gives the velocities of fluid (1) only. This figure shows an excellent agreement between the full three-dimensional Stokes problem and the two-dimensional Hele-Shaw model. The largest difference occurs at the interface ($y = 0$). The maximum relative error is 6.4%. This result encourages us to use the model for the analysis of more complex situations not amenable to three-dimensional analytic treatment.

For later use we calculate the volume fluxes of both liquids across the y-axis as

$$Q^{(1)} = \int_0^{\infty}\frac{\partial \Psi^{(1)}}{\partial y}\mathrm{d}y = Q^{(2)} = \int_{-\infty}^{0}\frac{\partial \Psi^{(2)}}{\partial y}\mathrm{d}y = -\frac{1}{12},$$

or in dimensional form

$$Q^{(1)} = Q^{(2)} = -\frac{\gamma\beta\, h^3}{12(\mu^{(1)}+\mu^{(2)})}.$$

The solution for the linear interface together with the expression for the volume flux provides us with all ingredients necessary for a qualitative understanding of

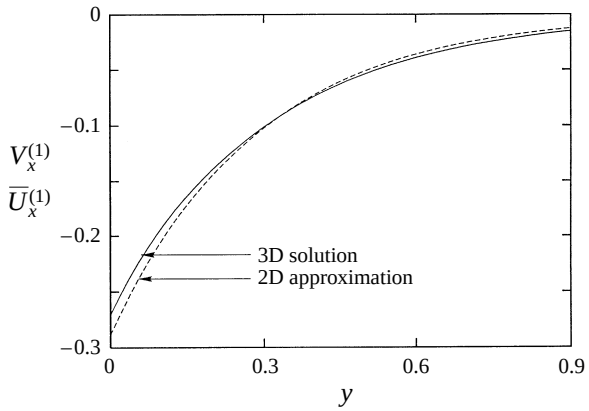

FIGURE 2. Flow at the linear interface: comparison of the velocity given by the two-dimensional Hele-Shaw model (dashed line) with a solution of the three-dimensional linear problem (solid line).

thermocapillary convection in arbitrarily complex geometries. For objects with lateral size L much larger than h, the thermocapillary forces penetrate only in a boundary layer with thickness of the order h and create jet-like flows with intensity proportional to the component of the temperature gradient along the interface. Since for a curved interface this intensity varies from point to point, the flow rate Q within the boundary layer will in general not be constant. By continuity, however, any variation $\mathrm{d}Q/\mathrm{d}s$ entails injection of fluid (or suction) into the bulk of the fluid. This phenomenon will be illustrated in the next section.

4.2. *Circular bubbles and droplets*

In this case it is convenient to use polar coordinates (r, φ) with the origin located at the centre of the drop and the polar axis directed in the direction of temperature gradient. As the characteristic length we take the radius of the droplet $L = R$. Then the curvature is constant ($K = 1$), and the coordinates (r, φ) are related to the coordinates (ξ, η) through the conditions $\xi = \varphi, \eta = 1 - r$. The curvilinear scale factor is $\ell = 1 - \eta = r$. From (3.11) the well-known relations between the components of the velocity and the streamfunction $v_\varphi = -\partial\Psi/\partial r$, $v_r = r^{-1}\partial\Psi/\partial\varphi$ can be obtained. The circular problem is thus governed by the equation

$$\left(\frac{1}{r}\frac{\partial}{\partial r}r\frac{\partial}{\partial r} - \frac{1}{r^2}\frac{\partial^2}{\partial\varphi^2}\right)\left(\frac{1}{r}\frac{\partial}{\partial r}r\frac{\partial}{\partial r} - \frac{1}{r^2}\frac{\partial^2}{\partial\varphi^2} - k^2\right)\Psi = 0, \tag{4.14}$$

and the boundary conditions at $r = 1$

$$\Psi^{(1)} = \Psi^{(2)} = 0, \tag{4.15}$$

$$\frac{\partial\Psi^{(1)}}{\partial r} = \frac{\partial\Psi^{(2)}}{\partial r}, \tag{4.16}$$

$$\hat{\mu}r\frac{\partial}{\partial r}\frac{1}{r}\frac{\partial\Psi^{(1)}}{\partial r} - (1-\hat{\mu})r\frac{\partial}{\partial r}\frac{1}{r}\frac{\partial\Psi^{(2)}}{\partial r} = \sin(\varphi). \tag{4.17}$$

The solution to this system can be evaluated in a straightforward manner as

$$\Psi^{(1)} = A_1\left\{\frac{I_1(kr)}{I_1(k)} - r\right\}\sin(\varphi), \tag{4.18}$$

$$\Psi^{(2)} = A_2 \left\{ \frac{K_1(kr)}{K_1(k)} - \frac{1}{r} \right\} \sin(\varphi), \tag{4.19}$$

where I_n, K_n are modified Bessel functions of first and second kind of order n respectively, and A_1, A_2 are constants, which are determined by the boundary conditions (4.15)–(4.17) and are given by

$$A_1 = -I_1(k)K_0(k)/C, \tag{4.20}$$

$$A_2 = I_2(k)K_1(k)/C, \tag{4.21}$$

$$C = \hat{\mu}(k^2 I_1(k) - 2kI_2(k))K_0(k) + (1-\hat{\mu})(k^2 K_1(k) + 2kK_0(k)I_2(k)). \tag{4.22}$$

Before we analyse this solution, it is useful to notice that the viscosity ratio does not enter the functional dependence of the flow field. It appears only in the multiplier common to both flows. This can be easily understood by observing that the continuity of the tangential velocity $v^{(1)} \sim v^{(2)}$ together with the estimate $\mu^{(1)}v^{(1)}/h + \mu^{(2)}v^{(2)}/h \sim \gamma\beta$ originating from boundary condition (3.20) imply that the velocity in both fluids is of the same order $v \sim \gamma\beta h/\mu_{max}$ where μ_{max} denotes the viscosity of the more viscous fluid. Notice that the functional form of the solution of the classical problem for thermocapillary motion in spherical droplets (Young *et al.* 1959) does not depend on the viscosity ratio either.

We now discuss the question of how the solution depends on the parameters. The dependence on the parameter $\hat{\mu}$ is trivial, therefore it is sufficient to consider the two limiting cases, $\hat{\mu} = 1$ and $\hat{\mu} = 0$ corresponding to a drop and a bubble, respectively. In figure 3(*a*) the streamfunction inside a droplet is plotted for $k = 2\sqrt{12}$. In the vicinity of the interface the fluid flows in the direction of decreasing temperature. The fluid returns in the core of the droplet. As a result, inside the droplet we have two vortices which are symmetric relative to the temperature gradient. In figure 3(*b*) we show the vorticity $\Omega = -\Delta\Psi$ corresponding to the flow in figure 3(*a*). If we fix the height of the cell h and enlarge the radius of the droplet, the parameter k becomes larger. One can see that for large aspect ratios the vorticity is very small in the core but strong at the interface. The largest values of Ω and of the velocity are at the interface, where the tangent vector of the interface is parallel to the temperature gradient. At these points the largest Marangoni forces are generated (see (3.28)). As k increases the boundary layer at the interface becomes thinner and the return flow aligns with the temperature gradient (figure 3*c*).

The observed evolution of the flow field with increasing k is in agreement with the qualitative picture drawn on the basis of the solution for the linear interface. As the aspect ratio of the drop increases, the action of the thermocapillary forces becomes confined to the boundary layer with thickness of the order $\delta \sim k^{-1}$ in the vicinity of the interface. Within this thermocapillary boundary layer strong vorticity gradients exist as a result of the shear stress. The role of the boundary layer consists in pumping fluid from the hot end of the bubble towards the cold end and in ejecting the fluid into the volume. For $k \gg 1$ the core flow is close to potential flow driven by the 'input' provided from the boundary layer, as can be seen in figure 3(*d*).

Figure 4 illustrates the flow structure outside a bubble, with $\hat{\mu} = 0$. Again we observe thin boundary layers at the interface and return flow in the core. The behaviour of the flow with increasing k is similar to the first case. However, the return flow does not become parallel to the temperature gradient. The boundary layers visible in figure 4 are strikingly similar to recent experimental findings of Bush (1997) who observed 'edge jets' at a bubble–air interface in a Hele-Shaw cell. In contrast to our case, these

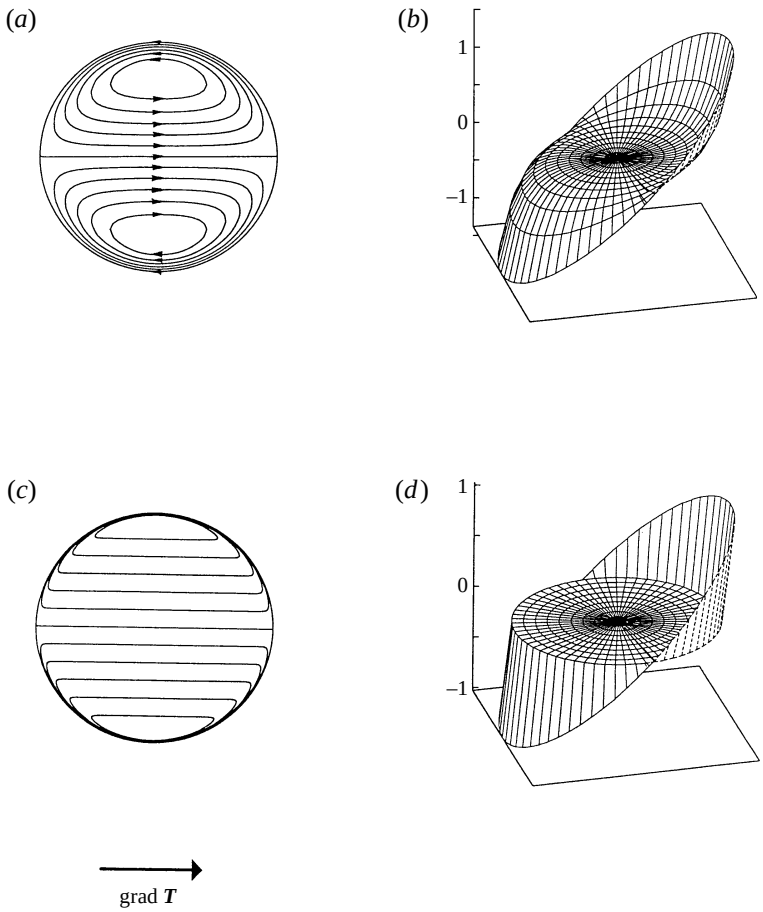

FIGURE 3. Analytic solutions for a circular drop: (a, c) isolines of streamfunction $\Psi^{(1)}$ ($\hat{\mu} = 1$) for different values of k: (a) $k = 2\sqrt{12}$; (c) $k = 20\sqrt{12}$ and (b, d) vorticity $\Omega^{(1)} = -\Delta\Psi^{(1)}$ for the same values of k as (a, c).

jets were driven by an inhomogeneous surfactant distribution, produced by a three-dimensional rolling motion of the bubbles. Nevertheless, it is remarkable that the present simple two-dimensional model can qualitatively capture these observations.

5. Asymptotic solution

As we have seen above, by increasing k the thickness of the thermocapillary boundary layer tends to zero as $\delta \sim k^{-1}$, and the vorticity of the core flow becomes very small. It is then natural to attempt the construction of an asymptotic theory for $k \to \infty$ using matched asymptotic expansions. In our explanation we shall closely follow Bender & Orszag (1978), omitting all details and representing only the main steps. To obtain solutions of the system (3.25) with boundary conditions (3.26)–(3.29) in the limit $k \to \infty$ we split each fluid in two regions, namely the boundary layer $|\eta| < \delta$ and the core $|\eta| > \delta$. Quantities referring to each region will be denoted by subscripts l, c respectively. Equations which describe the flow in each region are obtained from the governing equation (3.25). To examine the boundary layers we use the curvilinear coordinate system (ξ, η) and introduce the stretched boundary layer

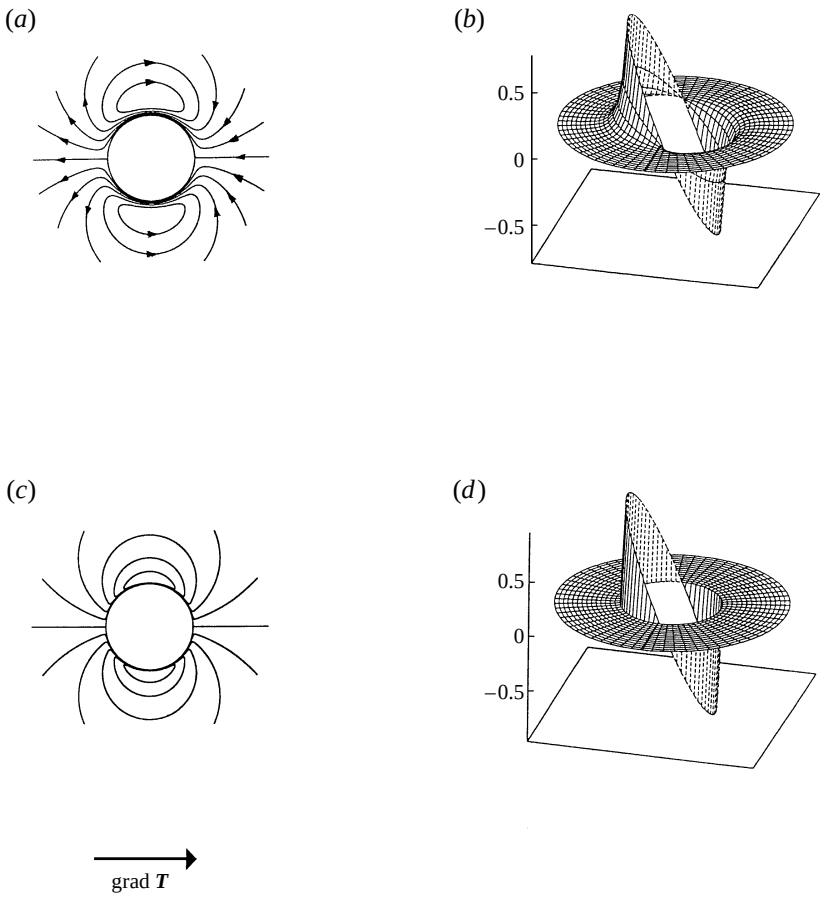

FIGURE 4. Analytic solutions for a circular bubble: (a, c) isolines of streamfunction $\Psi^{(2)}$ ($\hat{\mu} = 0$) for different values of k: (a) $k = 2\sqrt{12}$; (c) $k = 20\sqrt{12}$ and (b, d) vorticity $\Omega^{(2)} = -\Delta\Psi^{(2)}$ for the same values of k as (a, c).

coordinate $\zeta = k\eta$. Using the representation of the Laplace operator given in (3.12), substituting the new coordinate ζ, dividing by k^4, and taking the limit $k \to \infty$, we obtain to leading order the boundary layer equation

$$\frac{\partial^4 \Psi_l}{\partial \zeta^4} - \frac{\partial^2 \Psi_l}{\partial \zeta^2} = 0. \tag{5.1}$$

In writing this formula it is assumed that $\lim_{k\to\infty} K/k = 0$ which means that the interface has no curvature singularities. The general solution of equation (5.1) for each fluid is

$$\Psi_l = B_1 + B_2\zeta + B_3 e^{\zeta} + B_4 e^{-\zeta}, \tag{5.2}$$

where the unknown coefficients are functions of the 'slow' coordinate ξ along the interface. The requirement that $\Psi_l^{(1)}$ must remain finite in the limit $\zeta \to \infty$ and $\Psi_l^{(2)}$ in the limit $\zeta \to -\infty$ together with the boundary conditions (3.26)–(3.29) determine the unknown parameters as

$$B_2^{(1)} = B_2^{(2)} = B_3^{(1)} = B_4^{(2)} = 0, \quad B_1^{(1)} = -B_4^{(1)},$$
$$B_1^{(2)} = -B_3^{(2)}, \quad B_3^{(2)} = -B_4^{(1)}, \quad B_4^{(1)} = k^{-2}(\boldsymbol{\tau} \cdot \boldsymbol{t}).$$

In writing $B_4^{(1)}$ we have neglected terms of higher order than k^{-2}. If we denote $B_4^{(1)}$ as C and return to the coordinate η, then the streamfunctions of the boundary layer solutions are

$$\Psi_l^{(1)} = C\left(\mathrm{e}^{-k\eta} - 1\right), \tag{5.3}$$

$$\Psi_l^{(2)} = C\left(1 - \mathrm{e}^{k\eta}\right). \tag{5.4}$$

Notice that the boundary layer solution is entirely determined by the temperature field at the interface. Moreover, the functional dependence of the streamfunction on the transverse coordinate η is identical to that of the linear-interface solution with the effective temperature gradient $\boldsymbol{\tau} \cdot \boldsymbol{t}$. Far away from the interface, i.e. for $\eta \gg k^{-1}$, the boundary layer solution tends to its core value

$$\Psi_{lc}^{(1)} = -C(\xi), \tag{5.5}$$

$$\Psi_{lc}^{(2)} = +C(\xi), \tag{5.6}$$

which depends only on the arclength coordinate.

After having evaluated the boundary layer solution, we turn to the consideration of the core region. Taking the limit $k \to \infty$ in (3.25) we obtain Laplace's equation

$$\Delta \Psi_c = 0. \tag{5.7}$$

As expected from observation of figures 3(*d*) and 4(*d*), this equation describes potential flow, i.e. a flow whose vorticity $\Omega_c = -\Delta \Psi_c$ is zero. The boundary conditions for the core flow at the interface must be determined from the matching condition $\Psi_{cl} = \Psi_{lc}$. These conditions (Bender & Orszag 1978) require that Ψ_{cl} – the core solution evaluated at the interface – be equal to the continuation Ψ_{lc} of the boundary layer solution into the core, given by (5.5), (5.6). Mathematically, these conditions are expressed as

$$\Psi_{cl} = \mp C(\xi), \tag{5.8}$$

where the upper sign corresponds to the streamfunction for fluid (1) and the lower sign to the streamfunction for fluid (2). In addition, the Gauss condition

$$\int_\Gamma \partial_\eta \Psi_c \, \mathrm{d}\Gamma(s) = 0, \tag{5.9}$$

has to be satisfied for fluids forming a simply connected domain. A composite solution

$$\Psi_a = \Psi_c \pm C\mathrm{e}^{\mp k\zeta}, \tag{5.10}$$

which approximates the exact solution over the whole area can be obtained by adding to the core solution, the exponential part of the boundary layer solution, where subscript a means approximate solution.

In summary, the Laplace equation (5.7) together with the Dirichlet boundary condition (5.8) determine the core flow solutions in both fluids. The physical meaning of this system can be most easily understood by reformulating the asymptotic theory in terms of the velocity potential Φ_c defined by $v_\xi = \ell^{-1}\partial\Phi_c/\partial\xi$, $v_\eta = \partial\Phi_c/\partial\eta$. Using the incompressibility constraint and the relation $\partial\Psi_c/\partial\xi = -\ell\,\partial\Phi_c/\partial\eta$ which follows from (3.11) in the limit $k \to \infty$ we obtain the equation

$$\Delta \Phi_c = 0, \tag{5.11}$$

with the boundary condition

$$\frac{\partial \Phi_c}{\partial \eta} = \pm \frac{1}{k^2} \frac{\partial}{\partial \xi}(\boldsymbol{\tau} \cdot \boldsymbol{t}). \tag{5.12}$$

Point	$\Delta\Psi$ for $k = 5\sqrt{12}$	$\Delta\Psi$ for $k = 10\sqrt{12}$
$r = 0.5;\ \varphi = \pi/2$	0.10574	0.05510
$r = 0.5;\ \varphi = \pi/3$	0.10539	0.05525
$r = 0.5;\ \varphi = \pi/6$	0.10555	0.05532
$r = 0.75;\ \varphi = -\pi/6$	0.10299	0.05533
$r = 0.75;\ \varphi = -\pi/3$	0.10329	0.05534
$r = 0.75;\ \varphi = -\pi/2$	0.10332	0.05519

TABLE 1. The exact values for some internal points are compared with asymptotic values for $k = 5\sqrt{12}$, $k = 10\sqrt{12}$, where $\Delta\Psi = (\Psi^{(1)} - \Psi_a^{(1)})/\Psi^{(1)}$.

This boundary condition expresses that the normal velocity of the core flow at the interface is equal to the rate of change of the volume flux through the thermocapillary boundary layer.

Before engaging in a numerical treatment of the asymptotic system, we wish to demonstrate for the example of a circular drop that the boundary layer theory indeed provides an accurate approximation to the exact solution.

In the special case of the circular bubble or droplet we can easily determine the asymptotic solution of equation (5.10) as

$$\Psi_a^{(1)} = k^{-2}\left[r - \mathrm{e}^{k(r-1)}\right]\sin(\varphi), \tag{5.13}$$

$$\Psi_a^{(2)} = k^{-2}\left[\mathrm{e}^{k(1-r)} - \frac{1}{r}\right]\sin(\varphi). \tag{5.14}$$

The same expansions would have been obtained from solutions (4.18), (4.19) using the asymptotic behaviour of modified Bessel functions for large arguments $I_1(kr) \sim \exp(kr)/(2\pi kr)^{1/2}$, $K_1(kr) \sim \exp(-kr)(\pi/2kr)^{1/2}$ (Abramowitz & Stegun 1984). In table 1 the values of $\Psi_a^{(1)}$ are compared with the exact values $\Psi^{(1)}$ from (4.18) for two values of the parameter k. Notice that the asymptotic solution is independent of the parameter $\hat{\mu}$ and is already a good approximation for $k = 3\sqrt{12}$.

6. Numerical solution by a boundary element method

We have shown in the previous section that the flow in the core area for $k \gg 1$ is determined by the system

$$\Delta\Psi = 0, \tag{6.1}$$

$$\Psi = \mp(\boldsymbol{\tau}\cdot\boldsymbol{t}) \quad \text{at the interface } \Gamma. \tag{6.2}$$

Here we use the scaled streamfunction $\Psi = k^2\Psi_c$. In the boundary condition the upper sign corresponds to the streamfunction for fluid 1 and the lower sign to the streamfunction for fluid 2, $\boldsymbol{\tau}$ is the tangent vector to the interface Γ and $\boldsymbol{t}$ is the unit vector in the direction of the temperature gradient.

Here we notice that by using the method of matched asymptotic expansions we have transformed the problem from a fourth-order differential equation (3.25) with boundary conditions (3.26)–(3.29), to a Laplace's equation (6.1) with Dirichlet boundary condition (6.2) for return flow. Both systems have no analytic solution for droplets with complex shape, so that a numerical method must be invoked. However, Laplace's equation is much simpler to solve than the original problem. Therefore, we shall discuss a numerical method for the solution of the system (6.1), (6.2) in a complex geometry.

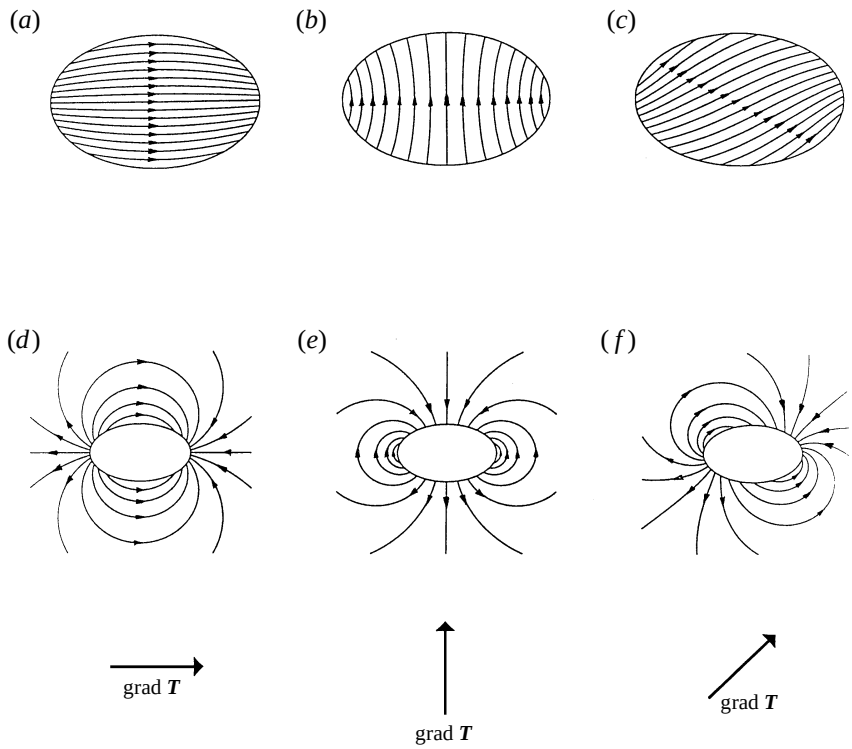

FIGURE 5. Isolines of the function Ψ_c inside and outside an elliptic droplet with eccentricity $e^2 = 0.6$ for three directions of the temperature gradient: (a, d) horizontal; (b, e) vertical; (c, f) diagonal.

We chose the boundary element method for it is comparatively simple, provides a good approximation and permits an efficient numerical implementation because the solution in an area can be expressed in terms of its boundary values at the contour Γ. With it the area need not be discretized but only the contour. The method is thoroughly described by Brebbia, Telles & Wrobel (1984) and will not be repeated here: therefore we go straight to discussion of the numerical results.

We investigate thermocapillary flows inside and outside droplets whose interface Γ in polar coordinates is given by the two-parameter family

$$r^2 = \frac{1}{1 - e^2 \cos^2(m\varphi)}. \tag{6.3}$$

If $m = 1$ the curve represents an ellipse with eccentricity e. For $m \geqslant 2$ equation (6.3) describes a 'starfish' with $2m$ rays and the parameter e determines size of the rays. As we have seen in §4, the function Ψ represents the core flow. Therefore we shall discuss the results only for this part of the asymptotic solution. Figure 5(*a–c*) shows the core flow inside an elliptical droplet ($\hat{\mu} = 1, \quad e^2 = 0.6$) for three directions of the temperature gradient. One can see that the flow is no longer parallel to the temperature gradient but depends on its direction. If the temperature gradient is directed along the longer axis of the ellipse, then streamlines are curved outwards (figure 5*a*). Conversely, if the temperature gradient is directed along the smaller axis of the ellipse then the streamlines are curved inwards the axis (figure 5*b*). Both effects become more pronounced as the eccentricity e is increased. For the case of a diagonal

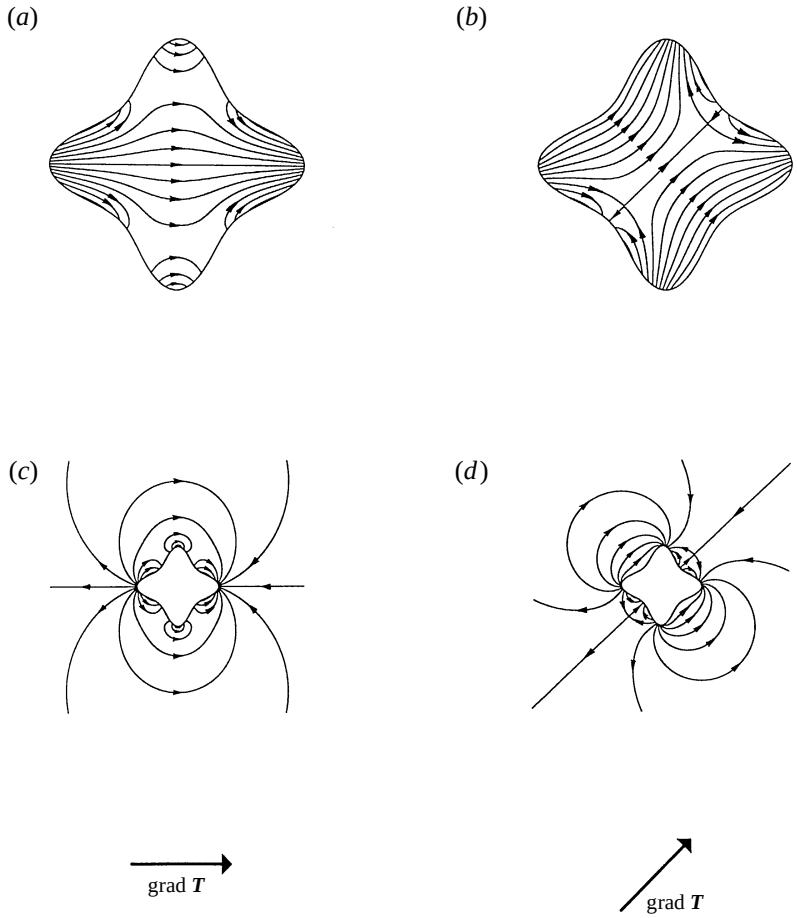

FIGURE 6. Isolines of the function Ψ_c inside and outside a 'starfish' with four rays ($m = 2, e^2 = 0.6$) for temperature gradients in the directions of the symmetry axes of curve Γ : (*a*,*c*) horizontal, (*b*,*d*) diagonal.

temperature gradient (figure 5*c*) the flow is no longer symmetric to the temperature gradient vector.

Figure 5(*d*–*f*) shows the function $\Psi^{(2)}$ ($\hat{\mu} = 0, \quad e^2 = 0.6$) outside an elliptical bubble. If ∇T is directed along the symmetry axis of the ellipse (figure 5*d*,*e*), then the return flow shows similar behaviour as for circular bubbles (compare with figure 4*c*). However, if a diagonal temperature gradient is applied, then the centre of the streamlines is shifted towards the longer axis of the ellipse, with increasing eccentricity e (figure 5*f*).

Figure 6(*a*,*b*) shows the functions $\Psi^{(1)}$ for $m = 2$ and temperature gradient in the direction of the symmetry axes of the curve. Here we see that in a finger, parallel to ∇T, Marangoni forces produce an intensive flow. In contrast, in a finger perpendicular to ∇T the fluid is almost at rest (figure 6*a*).

The streamfunction outside the 'starfish' bubbles is more complicated (figure 6*c*,*d*). In all cases one can see that the streamlines are compressed in regions of large interface curvature. In such regions the Marangoni force changes rapidly, generating large velocity gradients.

7. Moving interfaces

After having elucidated the structure of flows with pinned interfaces, it is desirable to understand the system in the case when movements of the interface are allowed. The general moving-boundary problem for thermocapillary Hele-Shaw convection is nonlinear and can be described by two different models. The first is if one fluid is completely enclosed by the other (see figure 1*b*). Here two thin films are formed at the top and bottom plates. These films are very thin compared to the cell height. But in this case thermocapillary forces act on all sides of the droplet including the top and bottom. In such a case the flow near the interface cannot be assumed to be a Poiseuille flow and our theory is not applicable to this model. In the second model (figure 1*c*) both fluids touch the plates. Here the assumption on the Poiseuille flow is valid; however, the moving-interface problem involves complex small-scale phenomena in the vicinity of the contact lines (see e.g. Dussan V. 1979; Carles *et al.* 1990) which are beyond the scope of the present work. As a first step we shall therefore restrict our attention to small displacements from equilibrium shape by analysing the stability of an interface under an applied temperature gradient. More specifically, we look for surface-wave instabilities in a Hele-Shaw cell for a semi-infinite fluid bounded by a free surface. In contrast to our previous analysis we assume that the contact lines are not fixed to the plates and the surface is free to move. Physically it may be identified with the limiting case of non-wetting fluid on an ideal even plate. For our theoretical explanations we choose Cartesian coordinates with the x-axis along the undisturbed surface as in §4.1. The perturbation of the surface from the mean position ($y = 0$) is determined by $y = A(x, t)$. The problem is governed by the equation (3.25), which with length scale $L = h$ takes the form

$$\Delta(\Delta - 12)\Psi = 0. \tag{7.1}$$

Since the surface is movable and consequently does not represent an isoline of the streamfunction the boundary condition (3.26) is not valid. Instead of this condition we must give a condition for the normal component of the surface stress. On the free surface this condition balances the surface tension times curvature. Together with the condition for shear stress (3.28), which balances the gradient of surface tension along the interface, it establishes a force acting on the free surface. This can be written in dimensionless form through the following vector equation (Pozrikidis 1992):

$$\boldsymbol{F} = \boldsymbol{\sigma} \cdot \boldsymbol{n} = (\boldsymbol{t} \cdot \boldsymbol{x} - D)K(x)\,\boldsymbol{n} - (\boldsymbol{\tau} \cdot \boldsymbol{t})\,\boldsymbol{\tau} \quad \text{on} \quad y = A(x, t), \tag{7.2}$$

where we have substituted equations (2.1), (3.1). The parameter $D = \alpha_0/\gamma\beta h$ describes the change of the surface tension relative to the characteristic length. Following the order of approximation for the surface tension given in (2.1) we require the parameter to be large, $D \gg 1$. It denotes that the surface tension does not change much over h. The dynamics come into the system with the kinematic boundary condition at the free surface which in the form of the streamfunction can be written

$$\frac{\partial A}{\partial t} = -\frac{\partial \Psi}{\partial y}\frac{\partial A}{\partial x} - \frac{\partial \Psi}{\partial x} \quad \text{on} \quad y = A(x, t). \tag{7.3}$$

For the stability analysis it is convenient to decompose the streamfunction into two components, namely the streamfunction of the basic flow (ψ_0) and the streamfunction (ψ_1) of the perturbation. The whole streamfunction becomes the sum of both components

$$\Psi = \psi_0 + \psi_1.$$

7.1. *Temperature gradient across the surface*

In this subsection we analyse the surface-wave instabilities due to a temperature gradient with unit vector $\boldsymbol{t} = (0, \mp 1)$ across the surface which represent the Hele-Shaw analogue to the classical surface-tension-driven Bénard convection. Here the upper sign denotes heating the Hele-Shaw cell from the fluid side and cooling from the gas side. The lower sign denotes the reverse case. As a basic state we take the solution $\psi_0 = 0$ since applying the temperature gradients to the undisturbed flat surface does not produce a flow. Following the standard procedure of linear stability theory we apply to the surface a disturbance with infinitesimal amplitude ε and a wavelength l. In order to be consistent with the basic assumptions of our theory we require $l > h$. Furthermore we introduce normal modes

$$\psi_1(x, y, t) = \varepsilon H(y) \exp(\lambda t + \mathrm{i}qx), \tag{7.4}$$

$$A(x, t) = \varepsilon \exp(\lambda t + \mathrm{i}qx), \tag{7.5}$$

where λ is the growth rate and $q = 2\pi h/l$ is the dimensionless wavenumber of perturbations. With the condition for the wavelength l the wavenumber must belong to the interval $0 < q < 2\pi$. The governing equation (7.1) is already linear and the condition (7.2) can be written in a linear approximation as follows:

$$\boldsymbol{\sigma} \cdot \boldsymbol{N} = -D\, A_x''\, \boldsymbol{N} \pm A_x'\, \boldsymbol{T} \quad \text{on} \quad y = 0, \tag{7.6}$$

where $\boldsymbol{N} = (0, 1)$ and $\boldsymbol{T} = (1, 0)$. Substituting (7.4), (7.5) into (7.1), (7.6) and omitting terms with order higher than ε we obtain a system for the function $H(y)$:

$$H^{(4)}(y) - (12 + 2q^2)H''(y) + q^2(12 + q^2)H(y) = 0, \tag{7.7}$$

$$H'''(0) - (12 + 3q^2)H'(0) = \mathrm{i}q^3 D, \tag{7.8}$$

$$H''(0) + q^2 H(0) = \pm \mathrm{i}q. \tag{7.9}$$

In order to obtain the condition (7.8) we have taken the derivative with respect to x of the normal component of the surface stress and used the boundary condition (3.9) to eliminate the pressure. The kinematic condition takes the form

$$\lambda = -\mathrm{i}qH(0), \tag{7.10}$$

which leads to the expression for the growth rate λ of the disturbances

$$\lambda = \frac{6Dq^3}{2(q^3(12 + q^2)^{1/2} - q^4 - 12q^2 - 36)} \mp \frac{q^2(q^2 + 6 - q(12 + q^2)^{1/2})}{2(q^3(12 + q^2)^{1/2} - q^4 - 12q^2 - 36)}. \tag{7.11}$$

Both terms on the right-hand side are negative for all values of q from the interval $0 < q < 2\pi$. Therefore the basic state $\psi_0 = 0$ is stable to the infinitesimal surface deformations if the heating is applied from the gas side, corresponding to the positive sign in (7.11). If the system is heated from the fluid side (corresponding to the negative sign in (7.11)) the system becomes unstable ($\lambda > 0$) if D is smaller than the critical value

$$D_c = \frac{6 + q^2 - q(12 + q^2)^{1/2}}{6q}. \tag{7.12}$$

The stability diagram corresponding to the neutral curve (7.12) is shown in figure 7(*a*).

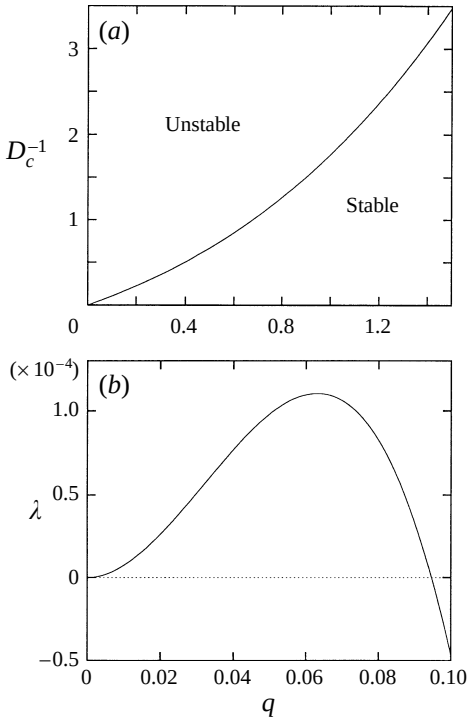

FIGURE 7. (*a*) Neutral stability curve of a flat interface heated from the fluid side. (*b*) Growth rate for $D = 10$.

Here we can see that for $D \gg 1$ the basic state becomes unstable for the long-wavelength perturbations. In this regime the amplitude of perturbations becomes larger and larger. Since the fluid is semi-infinite and there are no obstacles to the motion of the surface, the instability must lead to a fingering. It is similar to the interface instability in a Hele-Shaw cell observed by Saffman & Taylor (1958), where a less viscous fluid displaces a more viscous fluid. The physical mechanism of the instability (7.12) is very similar to that of long-wave instability in Bénard–Marangoni convection theoretically predicted by Scriven & Sternling (1964) and experimentally observed by VanHook *et al.* (1995). Indeed, a weak displacement of the interface towards the hot side creates a Marangoni flow which reinforces the 'erosion' of the interface. In contrast to the Bénard–Marangoni problem, however, the present long-wave instability cannot be supplanted by a short-wave instability because the temperature field does not change ($Pe \ll 1$). As a result, the Hele-Shaw geometry is well suited to studying the long-wave-instability in its pure form.

7.2. *Temperature gradient along the surface*

In this case the vector $\boldsymbol{t} = (1, 0)$ is directed along the x-axis. The basic state here is the steady-state solution for a linear interface (see §4.1). Then the whole streamfunction is given by

$$\Psi = \frac{1 - \mathrm{e}^{\sqrt{12}y}}{12} + \psi_1.$$

Analogously to the previous section we introduce normal modes (7.4), (7.5), and substitute them into the governing equation and the boundary conditions to obtain

the following system for the function $H(y)$:

$$H^{(4)}(y) - (12 + 2q^2)H''(y) + q^2(12 + q^2)H(y) = 0, \tag{7.13}$$

$$H'''(0) - (12 + 3q^2)H'(0) = \mathrm{i}q^3 D, \tag{7.14}$$

$$H''(0) + q^2 H(0) = \sqrt{12}. \tag{7.15}$$

Here it is assumed that the surface tension does not change much over l ($D \gg l$). The kinematic boundary condition becomes

$$\lambda = -\mathrm{i}q\left(H(0) - \frac{1}{\sqrt{12}}\right). \tag{7.16}$$

Since the perturbations will move with the basic flow, the complex eigenvalue λ can be decomposed into two components

$$\lambda = \lambda_r + \mathrm{i}\lambda_\mathrm{i},$$

where λ_r is the growth rate and λ_i is the phase speed of disturbances. A straightforward computation leads to the following expressions for λ_r and λ_i:

$$\lambda_r = \frac{3Dq^3}{q^3(12 + q^2)^{1/2} - q^4 - 12q^2 - 36}, \tag{7.17}$$

$$\lambda_i = \frac{q^2[(q^2 - 6)(12 + q^2)^{1/2} - q(q^2 + 6)]}{\sqrt{12}(q^3(12 + q^2)^{1/2} - q^4 - 12q^2 - 36)}. \tag{7.18}$$

An analysis of (7.17) shows that $\lambda_r < 0$. Therefore the basic flow is stable to small deformation of the surface for all values of $q = (0\text{–}2\pi)$. As a result, there is no counterpart to the hydrothermal-wave instability (Smith & Davis 1983) in a Hele-Shaw cell.

8. Conclusions

In this work we have investigated the thermocapillary flow in two immiscible fluids confined in a Hele-Shaw cell. The main results can be summarized as follows.

(1) The thermocapillary Hele-Shaw problem can be solved exactly for linear and circular interfaces. For a linear interface the flow is parallel to the interface and symmetric. For circular droplets there are two parameters which determine the structure of the flow: $\hat{\mu}$ which describes the ratio between the viscosities inside and outside the droplet and k which describes the relative aspect ratio.

(2) For large values of k an asymptotic theory can be obtained. This limit corresponds to large droplets. In this case the original problem can be transformed into Laplace's equation with a Dirichlet boundary condition which can be solved efficiently.

(3) For droplets with complex shapes the structure of the flow depends on the parameter k as well as on the droplet geometry and the direction of the temperature gradient.

(4) For a semi-infinite fluid bounded by a free movable surface a long-wavelength instability is predicted due to the temperature gradient across the surface when heating the Hele-Shaw cell from the liquid side and cooling from the gas side.

The present theory represents the minimal model of surface-tension-driven flow in a complex geometry. Although the theory is comparatively simple, its predictions, in particular the structure of the flow field in the interior of a drop, should be

amenable to experimental verification. Even if the flow is very slow due to the limited temperature gradient in an experiment, it has a cumulative effect on Lagrangian quantities such as the displacement of a tracer particle or a tiny spot of dye which grow linearly with time. Thus, after sufficiently long observation time Lagrangian displacements magnify to a macroscopic size L and become observable. For instance, the boundary layer velocity in a drop of silicone oil ($h = 1$ mm, $L = 10$ mm) exposed to a weak temperature gradient $\beta = 10$ K m^{-1} is as small as 0.063 mm s^{-1} which may appear unsettling at first glance. However, after an observation time of roughly 150 s, a particle will have travelled a distance of the order L.

Our theory defines a simple conceptual framework for the study of complex thermocapillary phenomena that would be difficult to investigate in the general three-dimensional setting. For instance, the two-dimensional Hele-Shaw geometry offers an attractive environment to study Marangoni convection in chemically reacting fluids or in fluids containing surfactants without the need to take into account the nonlinearity of the Navier–Stokes equation and the buoyancy force. In this context, it would be interesting to extend the experiments of Park, Maruvada & Yoon (1994) to the non-wetting case treated in the present paper.

Finally we want to discuss the behaviour of bubbles in a non-wetting fluid with a movable interface due to thermocapillary forces. The case of small circular non-deformable bubbles was considered theoretically by Siekmann (1979). Such bubbles move with a constant velocity U_m in the direction of the temperature gradient. The migration velocity decreases with increasing radius of the bubbles as $U_m \sim R^{-1}$. However, for increasing radius the capillary forces are not strong enough to fix the shape and the bubble cannot be assumed undeformable. In order to understand qualitatively the behaviour of large bubbles we cut the surface of the bubble into parts so that in each part the surface can be assumed linear. To the parts that are parallel to the temperature gradient the results from §7.2 can be applied. Here the surface is stable to small deformations. For the parts that are perpendicular to the temperature gradient there are two possibilities depending on the relative arrangement of fluid and gas phases with respect to the direction of the temperature gradient (see §7.1): the shape of the bubble at the cold side is stable to small surface deformations and becomes unstable at the hot side. Here the surface moving in the direction of the temperature gradient can develop a nose. Since the volume of a bubble is constant it can lead to singularities in the nose, similar to the studies by Almgren (1996).

We are grateful to Ch. Karcher and V. Galindo for useful discussions and to J. W. M. Bush for making available the manuscript (Bush 1997) prior to publication. One of us (W. B.) acknowledges the Sächsisches Staatsministerium für Wissenschaft und Kunst for financial support.

Appendix. Discussion of the thermal model

In this Appendix we wish to demonstrate that the deviation of the fluid temperature from the temperature gradient in the plates is of the same order as other effects neglected in the derivation of the Hele-Shaw model.

First we assume that the plates of the cell have infinite thermal conductivities and a linear temperature gradient is applied. Further it is assumed that the Péclet number of the fluids $Pe = uh/\kappa$, where κ is thermal diffusivity, is sufficiently small ($Pe \ll 1$). This condition expresses that the temperature in the fluids is predominantly

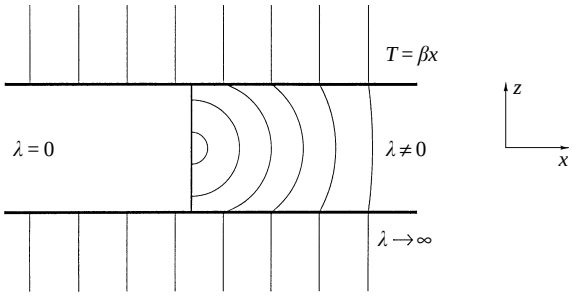

FIGURE 8. Sketch of the perturbed temperature distribution due to the finite heat conductivity of the fluid.

transported by diffusivity. This regime frequently arises in creeping flow. For our example with silicone oil NM10 with $h = 1$ mm and $\beta = 10$ K m^{-1} we have $Pe = 0.63$.

The effect of finite heat diffusivity of the fluids is to bend the temperature isolines. This is due to the fact that the fluids, separated by a linear interface $x = 0$, cannot at the same time possess a temperature distribution $T = \beta x$ and satisfy the condition $\lambda_1 \partial_x T_1 = \lambda_2 \partial_x T_2$ of heat flux continuity where λ_1 and λ_2 are the heat conductivities of the fluids. Obviously this effect is most strongly pronounced if the temperature gradient is perpendicular to the interface, and the effect does not exist if the temperature gradient is parallel to the interface. Therefore we shall consider the worst case, sketched in figure 8, where the temperature gradient is perpendicular and the left-hand fluid has zero heat conductivity.

The temperature distribution $T(x, z)$ in the right-hand fluid of figure 8 is described by the Laplace equation

$$\Delta T = 0, \tag{A 1}$$

and the boundary conditions

$$T(x, h/2) = T(x, -h/2) = \beta x, \tag{A 2}$$

$$\partial_x T(0, z) = 0. \tag{A 3}$$

The general solution to this equation which converges to βx as $x \to \infty$ and which is symmetric with respect to the mid-plane $z = 0$ is

$$T = \beta x + \sum_n G_n \exp(-k_n x) \cos(k_n z), \tag{A 4}$$

where β can be easily identified with the temperature gradient and G_n are constants, which must be determined from boundary conditions. From boundary condition (A 2) we conclude that $k_n = \pi(2n - 1)/h$ $(n = 1, 2, 3, \ldots)$. In order to satisfy the boundary condition (A 3) we evaluate $\partial_x T(0, z)$ as

$$\partial_x T(0, z) = \beta - \sum_{n=1}^{\infty} G_n k_n \cos(k_n z). \tag{A 5}$$

Using the identity

$$1 = \sum_{n=1}^{\infty} (-1)^{n+1} \frac{4}{\pi(2n-1)} \cos(k_n z) \tag{A 6}$$

we obtain the coefficients $G_n = (-1)^{n+1}4\beta h/[\pi^2(2n-1)^2]$. Substitution of these constants into the series of (A 4) and averaging over the height h lead to the inequalities

$$\frac{8\beta h}{\pi^3}\sum_{n=1}^{\infty}\frac{\exp(-k_n x)}{(2n-1)^3} \leqslant \frac{8\beta h}{\pi^3}\sum_{n=1}^{\infty}\frac{1}{(2n-1)^3} < \frac{\beta h}{\pi}.$$

With this, the average temperature in right-hand liquid is given by

$$\bar{T} \approx \beta x + \frac{\beta h}{\pi} = \beta x + O(h). \tag{A 7}$$

For small h the second term can be neglected, and the distribution of temperature in liquid (2) can be approximated by $\bar{T} = \beta x$ as can the distribution of temperature in the plates of the cell. Similar equations can be obtained if the thermal conductivities of both liquids are not zero. The fact that the temperature in the middle of the interface is higher leads to the generation of three-dimensional rolls. Since such a flow is directed towards the plates, it will tend to homogenize the temperature perturbation.

REFERENCES

Abramowitz, M. A. & Stegun, I. A. 1984 *Pocketbook of Mathematical Functions*. Harri Deutsch.

Almgren, R. 1996 Singularity formation in Hele-Shaw bubbles. *Phys. Fluids* **8**, 344–352.

Aris, R. 1989 *Vectors, Tensors and the Equations of Fluid Mechanics*. Dover.

Bender, C. M. & Orszag, S. A. 1978 *Advanced Mathematical Methods for Scientists and Engineers*. McGraw Hill.

Bensimon, D., Kadanoff, L. P., Liang, S., Shraiman, B. I. & Tang, C. 1986 Viscous flow in two dimensions. *Rev. Mod. Phys.* **58**, 977.

Bratuhin, J. K. 1975 Thermocapillary-driven motion of a viscose drop. *Meh. Gidk. i Gasa* **N5**, 156–161 (in Russian).

Bratuhin, J. K. & Zuev, A. L. 1984 Thermocapillary-driven motion of a bubble in horizontal Hele-Shaw cell. *Meh. Gidk. i Gasa* **N3**, 62–67 (in Russian).

Brebbia, C. A., Telles, J. C. & Wrobel, L. C. 1984 *Boundary Element Techniques*. Springer.

Bush, J. W. M. 1997 The anomalous wake accompanying bubbles rising in a thin gap: a mechanically forced Marangoni flow. *J. Fluid Mech.* **352**, 283–303.

Carles, P., Troian, S. M., Cazabat, A. M. & Heslot, F. 1990 Hydrodynamic fingering instability of driven wetting films: hindrance by diffusion. *J. Phys. Condensed Matter* **2**, SA477–SA482.

Davis, S. H. 1983 In *Waves on Fluid Interfaces* (ed. R. E. Meyer), p. 291. Academic.

Davis, S. H. 1987 Thermocapillary instabilities. *Ann. Rev. Fluid Mech.* **19**, 403–435.

Dussan V., E. B. 1979 On the spreading of liquids on solid surfaces: static and dynamic contact angles. *Ann. Rev. Fluid Mech.* **11**, 371–400.

Edwards, D. A., Brenner, H. & Wasan, D. T. 1991 *Interfacial Transport Processes and Rheology*. Butterworth Heinemann.

Ehrhard, P. & Davis, S. H. 1991 Non-isothermal spreading of liquid drops on horizontal plates. *J. Fluid Mech.* **229**, 365–388.

Galindo, V., Gerbeth, G., Langbein, D. & Treuner, M. 1994 Unsteady thermocapillary migration of isolated spherical drops in a uniform temperature gradient. *Microgravity Sci. Technol.* **VII/3**, 234–241.

Gennes, P. de 1985 Wetting: statics and dynamics. *Rev. Mod. Phys.* **57**, 827–863.

Grotberg, J. B. 1994 Pulmonary flow and transport phenomena. *Ann. Rev. Fluid Mech.* **26**, 529–571.

Hammerschmid, P. 1987 Bedeutung des Marangoni-Effekts für metallurgische Vorgänge. *Stahl und Eisen* **107**, 61–66.

Jensen, O. & Grotberg, J. B. 1992 Insolutable surfactant spreading on a thin viscous film: shock evolution and film rupture. *J. Fluid Mech.* **240**, 259–288.

Koschmieder, E. L. 1993 *Bénard Cells and Taylor Vortices*. Cambridge University Press.

Park, C. W., Maruvada, S. R. K. & Yoon, D. Y. 1994 *Phys. Fluids* **6**, 3267–3275.

Pozrikidis, C. 1992 *Boundary Integral and Singularity Methods for Linearized Viscous Flow*. Cambridge University Press.

Saffman, P. G & Taylor, G. I. 1958 The penetration of a fluid into a porous medium or Hele-Shaw cell containing a more viscous liquid. *Proc. R. Soc. Lond.* A **245**, 312–329.

Scriven, L. E. & Sternling, C. V. 1964 On cellular convection driven by surface-tension gradients: effects of mean surface tension and surface viscosity. *J. Fluid Mech.* **19**, 321–340.

Siekmann, J. 1979 On slow motion of a bubble in Hele-Shaw flow subject to a horizontal temperature gradient. *Acta Mechanica* **39**, 39–50.

Smith, M. K. & Davis, S. H. 1983 Instabilities of dynamic thermocapillary liquid layers. Part 2. Surface-wave instabilities. *J. Fluid Mech.* **132**, 145–162.

VanHook, S. J., Schatz, M. F. & McCormick, W. D. 1995 Long-wavelength instability in surface-tension-driven Bénard convection. *Phys. Rev. Lett.* **75**, 4397–4400.

Wilson, S. K. 1993 The steady thermocapillary-driven motion of a large droplet in a closed tube. *Phys. Fluids* A **5**, 2064–2066.

Young, N. O., Goldstein, I. S. & Block, M. I. 1959 The motion of the bubbles in a vertical temperature gradient *J. Fluid Mech.* **6**, 350–356.